HHS Public Access

Author manuscript

Adv Mater. Author manuscript; available in PMC 2022 September 01.

Published in final edited form as:

Adv Mater. 2021 September ; 33(35): e2102153. doi:10.1002/adma.202102153.

A Smartphone-Enabled Portable Digital Light Processing 3D Printer

Wanlu Li[‡],
Division of Engineering Medicine, Department of Medicine, Brigham and Women's Hospital, Harvard Medical School, Cambridge, MA 02139, USA

Mian Wang[‡],
Division of Engineering Medicine, Department of Medicine, Brigham and Women's Hospital, Harvard Medical School, Cambridge, MA 02139, USA

Luis Santiago Mille,
Division of Engineering Medicine, Department of Medicine, Brigham and Women's Hospital, Harvard Medical School, Cambridge, MA 02139, USA

Juan Antonio Robledo,
Division of Engineering Medicine, Department of Medicine, Brigham and Women's Hospital, Harvard Medical School, Cambridge, MA 02139, USA

Valentín Huerta,
Division of Engineering Medicine, Department of Medicine, Brigham and Women's Hospital, Harvard Medical School, Cambridge, MA 02139, USA

Tlalli Uribe,
Division of Engineering Medicine, Department of Medicine, Brigham and Women's Hospital, Harvard Medical School, Cambridge, MA 02139, USA

Feng Cheng,
Division of Engineering Medicine, Department of Medicine, Brigham and Women's Hospital, Harvard Medical School, Cambridge, MA 02139, USA

Hongbin Li,
Division of Engineering Medicine, Department of Medicine, Brigham and Women's Hospital, Harvard Medical School, Cambridge, MA 02139, USA

Jiaxing Gong,
Division of Engineering Medicine, Department of Medicine, Brigham and Women's Hospital, Harvard Medical School, Cambridge, MA 02139, USA

Terry Ching,
Division of Engineering Medicine, Department of Medicine, Brigham and Women's Hospital, Harvard Medical School, Cambridge, MA 02139, USA

[*] yszhang@research.bwh.harvard.edu, khoon.lim@otago.ac.nz.
[‡]Wanlu Li and Mian Wang contributed equally to this work

Supporting information
Supporting Information is available from the Wiley Online Library or from the author.

Caroline A. Murphy,
Christchurch Regenerative Medicine and Tissue Engineering (CReaTE) Group, Department of Orthopaedics Surgery and Musculoskeletal Medicine, University of Otago Christchurch, Christchurch 8011, New Zealand

Ami Lesha,
Division of Engineering Medicine, Department of Medicine, Brigham and Women's Hospital, Harvard Medical School, Cambridge, MA 02139, USA

Shabir Hassan,
Division of Engineering Medicine, Department of Medicine, Brigham and Women's Hospital, Harvard Medical School, Cambridge, MA 02139, USA

Tim Woodfield,
Christchurch Regenerative Medicine and Tissue Engineering (CReaTE) Group, Department of Orthopaedics Surgery and Musculoskeletal Medicine, University of Otago Christchurch, Christchurch 8011, New Zealand

Khoon S. Lim*,
Christchurch Regenerative Medicine and Tissue Engineering (CReaTE) Group, Department of Orthopaedics Surgery and Musculoskeletal Medicine, University of Otago Christchurch, Christchurch 8011, New Zealand

Yu Shrike Zhang*
Division of Engineering Medicine, Department of Medicine, Brigham and Women's Hospital, Harvard Medical School, Cambridge, MA 02139, USA

Abstract

Three-dimensional (3D) printing has emerged as an enabling approach in a variety of different fields. However, the bulk volume of printing systems limits the expansion of their applications. In this study, a portable 3D digital light processing (DLP) printer is built based on a smartphone-powered projector and a custom-written smartphone-operated App. Constructs with detailed surface architectures, porous features, or hollow structures, as well as sophisticated tissue analogues, are successfully printed using this platform, by utilizing commercial resins as well as a range of hydrogel-based inks, including poly(ethylene glycol)-diacrylate (PEGDA), gelatin methacryloyl (GelMA), or allylated gelatin (GelAGE). Moreover, due to the portability of our unique DLP printer, medical implants can be fabricated for point-of-care usage, and cell-laden tissues can be produced in situ, achieving a new milestone for mobile-health technologies. Additionally, the all-in-one printing system described herein enables the integration of the 3D scanning smartphone App to obtain object-derived 3D digital models for subsequent printing. Along with further developments, we anticipate this portable, modular, and easy-to-use smartphone-enabled DLP printer to secure exciting opportunities for applications in resource-limited and point-of-care settings not only in biomedicine but also for home and educational purposes.

Keywords

digital light processing; 3D printing; bioprinting; smartphone; portable

Three-dimensional (3D) printing as an additive manufacturing technique used towards fabricating user-defined structures, has been implemented in a range of different fields, including manufacturing, food engineering, and biomedical applications.[1] With the intriguing development of materials science, as well as the hardware and software upgrades of printing systems, we are witnessing an expansion in utilization of 3D printing technologies into more areas.[2] However, limitations in the current 3D printing systems are their bulky volume and footprint, which results in inconvenient operational processes, hindering the availability of this technology in resource-limited or point-of-care settings. It should also be noted that very little optimization work has been carried out on developing easy-to-use software of current 3D printing platforms for wide adaptability with increasingly popular, smart digital devices. Therefore, there is an urgent need to build a portable and modular 3D printer suitable for laboratory, industrial, and personal demands.

To achieve this goal, we hypothesized that the smartphone could serve as an ideal interface for a portable 3D printer, inspired by its continuous innovations in computing power and imaging/sensing capacities suited for a range of healthcare applications.[3] It has been demonstrated that phone-associated systems can achieve field-portability and point-of-care convenience. For instance, a smartphone-based microscope was developed as a portable optical imaging tool for in situ DNA detection, allowing on-site patient diagnosis.[4] As another example, a chemical sensing platform developed on the smartphone was accomplished by incorporating chemoresponsive nanomaterials into the circuity of nearfield communication tag on the smartphone, in an inexpensive way.[5] There are numerous advantages of using a smartphone as the controlling tool or the signal-readout platform, which might be helpful for printer implementation. The Bluetooth/WiFi communication possibilities, the CPU, and the storage space are intrinsically integrated into smartphones, opening the opportunities of acting as the data-processing platform. Another crucial feature of modern smartphones is the touchscreen that cannot be overlooked, providing an accessible software user interface for 3D printing. Furthermore, facilitated by existing Apps for 3D model design and the high-quality cameras on smartphones, the required digital models of 3D printing can be readily obtained on-demand in addition to open-source computer-aided designs.

3D printers based on vat-polymerization methods, including stereolithography apparatus (SLA) and digital light processing (DLP), were traditionally used for resin printing to create prototypes.[6] Recently, considerable research efforts have been devoted to applying the vat-polymerization approach for biomedical applications attributed to their ability to produce sophisticated architectures.[7] Unlike SLA using point laser scanning, DLP relies on projection of planar digital light patterns to fabricate 3D constructs in a layer-by-layer manner, which makes the process significantly faster than many other printing strategies.[8] Furthermore, the accessibility to DLP hardware, such as commercial projectors as light sources, places DLP as a desirable choice for building new light-based 3D printers. Besides, by adoption visible-light photoinitiators,[9] the visible light-assisted DLP printing process is a safer choice for biofabrication of cell-laden constructs and higher-throughput 3D in vitro tissue models compared with ultraviolet (UV)-based photopolymerization.

In this study, we first described the development of a portable and modular DLP 3D printer based on a smartphone-powered projector and operated using a custom-written smartphone App, with total dimensions of 10 cm × 20 cm × 20 cm in width, length, and height, respectively (Figure 1a and b, inclusive of the motor, the build platform, the vat, the optical system, and the smartphone-powered projector). Particular emphasis was placed on developing comparable printing resolution with commercial DLP printers despite the significantly lower costs (excluding the smartphone). This was followed by validating the printing competency with both commercial resins and hydrogel (bio)inks. Finally, we explored the feasibility of the developed smartphone-enabled 3D printing system in the fabrication of medical implants, as well as in situ bioprinting. Also of critical importance, this system offered the possibility of integrating a scanning App for acquisition of 3D models into the established printing system, facilitating on-demand applications.

As shown in Figure 1a, the smartphone-enabled DLP printer typically involves a smartphone-powered projector for outputting the designed patterns, with a built-in customized smartphone App to control the system. To make it more affordable for general use, the implementation of cost-effective hardware would be decisive (since smartphones are commonplace nowadays and readily available anywhere and thus not included in the cost analysis). Therefore, the materials adopted to build the printer, as well as manufacturing methods, were low-cost and conveniently accessible (material information and costs listed in Table S1). Details of the printer assembly are described in the Supporting Information and is schematized in Figure S1.

It is worthwhile mentioning that the area and volume of the vat at 3.14 cm^2 and 3.77 mL, respectively, were made relatively small as the overarching goal of the device was not to print large-scale objects although scaling-up is easy. In addition, the system was assembled to allow the lenses and the polymerization vat to be adjusted across different levels, adding versatility to the printing system. For instance, it allowed lenses with different focal lengths to be switched, resulting in different magnifications and light intensities at the bottom of the vat. This design thus has exhibited significant potential for printing structures with flexibility over multiple length scales. Complete details of this feature are provided in the final proof-of-concept examples, and only the lens with 10 cm of focal length was used as the standard optics in the other sections of this work.

The design of this smartphone-enabled DLP printer harnessed a small, smartphone-powered, yet powerful projector (G6S DLP Pocket Projector/Mini Projector, IMEGO) as the light source and pattern-generator, allowing the printer to be controlled directly by a smartphone. Patterns generated from the projector were irradiated onto a silver front-coated optical mirror, which was positioned in front of the projector with a 45°-angle, 38 mm away from the projector lens (Figure 1ci). As a result, the light bounced straight up at 90° and was forced into a convex lens placed 66 mm away from the mirror. Then, the images went through the biconvex lens (10-cm focal length) and were focused onto the vat located 72.8 mm above. Finally, a Teflon AF2400 film (50-μm thickness, Random Technologies) was placed at the bottom of the vat to allow a clear transmission of light with the least attenuation (>95% light transmittance), as well as to provide an oxygen-permeable window for reducing material adhesion.[10] Notably, the size of the projected pattern was decreased

to 10 times at the vat as compared with the original projected size. The method of optical calculation is discussed in the Supporting Information and illustrated in Figure 1cii and 1ciii. With these in mind, the projecting area at the location of the ink vat was calculated as 23.4 mm in width and 41.6 mm in length. Again, we demonstrated the proof-of-concept utility of our platform and hence chose this smaller working size to begin with. The maximum size of projected images can be easily tuned by replacing with another smartphone-powered projector that may provide larger projection areas, or properly selecting other optics that focus the light onto the vat. Meanwhile, the sizes of the build platform and the vat in our smartphone-enabled DLP printing system can be conveniently expanded as well, as the printing size is increased.

The characteristics of this smartphone-powered projector featured a liquid crystal display (LCD) screen (954 × 480 pixels) and the RGB (red, green, blue) light-emitting diode (LED) light source, which delivered light density up to 1,400 lumens, or 0.23 mW cm^{-2}, onto the vat area (Figure S2a). As an indicator of photopolymerization kinetics, the working curve implies the resin/ink behavior under specified photocuring conditions and provides a quick estimation of print settings.[11] The working curve was obtained by plotting irradiation dosage (exposure) and cure depth calculated via Equation 1, where irradiation dosage resulted from light intensity multiplied by exposure time, and cure depth directly measured from the optical microscopic image:

$$C_d = D_p \ \ ln\frac{E}{E_c} \tag{1}$$

where C_d is the cure depth, D_p is the light penetration depth, E is the irradiation dosage (exposure), and E_c is the energy required for achieving the gelation point. As shown in Figure S2b, for the ink of 40 v/v% poly(ethylene glycol)-diacrylate (PEGDA, molecular weight, M_w = 575 Da), the curing depths ranged from 0 μm to 500 μm. As an example of applying our smartphone-enabled DLP printer, a gyroid was fabricated using a commercial resin (Photocentric Daylight Firm Resin, MatterHackers), where Figure 1d illustrates the print fidelity achieved and a close match with the designed model. The printed gyroid featured 1-mm pore size and highly curved surfaces.

To reduce human interactions and avoid operation errors during printing, an automated control system was developed as illustrated in Figure 2a. Using an HC-06 Bluetooth module, the instructions were sent from the smartphone to the microcontroller, operating on the sensor and actuator in a master-slave fashion. The Arduino Mega board (ATMega 2560, Newark Electronics) was used as the central controller for the hardware. An easy-to-use smartphone App was custom-written as the primary interface between the user and the 3D printer to realize better operational performance. Relying on this uncomplicated and functional smartphone App, the touchscreen of smartphones made the operations easier in terms of model-slicing, pattern-adjusting, and parameter-choosing, even for users who may not be familiar with 3D modeling-slicing and 3D printing. The programming language is described in Supporting Information. As shown in the flow chart of Figure 2b, an exemplary smartphone, Samsung Galaxy S9 with Android Pie (version 9) was used to test the printing software and perform all printing tasks.

Once the Bluetooth-enabled device was found through the App, a main menu was displayed on the screen of the smartphone, showing five options ‘Print’, ‘Print High Viscosity’, ‘STL Slicer’, ‘Settings’, and ‘Exit’. Finally, the App sent the command of these options to the Arduino transceiver for obtaining the desired function. There were two different types of printing modes implemented in the App and supported by its algorithm for the motor movement and image display. Mode 2 (Print High Viscosity) added the step of moving to the maximum distance before going to the height of next layer compared with the Mode 1 (Print), with the aim of printing with viscous resins/inks. The ‘STL Slicer’ allowed the transformation of a 3D STL model into a series of 2D images directly in the smartphone App, which is unprecedented. It was created with the working principle of converting the STL model into a voxel representation, which was partitioned by layers as a grid of pixels (Figure 2c). Therefore, the number of images obtained was dependent on the model size, and the voxel number that the user chooses. A higher number of voxels could improve the quality of images but result in a large number of sliced images. This ‘STL Slicer’ function, as a key function developed in our smartphone App, enabled to achieve printing patterns without needing external web-based tools or software. Meanwhile, ‘Settings’ displayed instructions on scaling and rotating images, as well as adjusting the build platform position all attainable via the touchscreen of the smartphone.

A general and quick printing procedure of a gyroid structure using a commercial resin (Photocentric Daylight Firm Resin, also see Figure 1d) is presented in Movie S1 and Figure S3. Gyroid is featured with the intricate internal structure and has been applied in nanoporous membranes, photonic crystals, and biomimetic modeling.[12] In our demonstration, the gyroid 3D model (8 mm × 8 mm × 8 mm) was sliced before printing, and its size and position were adjusted based on the scale of background grids (1 mm × 1 mm). After setting the home position, exposure time, and layer thickness, the entire printing process finished in 12 min. The processing bar on the top of the smartphone screen indicated the print layer numbers and the remaining time. Overall, this smartphone-enabled printing system demonstrated significant promise in fabrication of complex 3D objects using a standardized workflow, all with the aid of the remotely controlled smartphone App.

The printability, fidelity, and resolution were subsequently evaluated for the smartphone-enabled printing platform, taking into account various properties, photoinitiator concentrations, and photoabsorber additives.[13] PEGDA, which is cytocompatible, has been widely used alone or in combination with other materials in DLP (bio)printing applications.[14] Therefore, single-layer printing experiments were carried out using PEGDA (M_w = 575 Da) with varying amounts of photoinitiator (tris(2,2’-bipyridyl)dichloro-ruthenium(II) hexahydrate with sodium persulfate, Ru/SPS) and photoabsorber (Ponceau 4R) to identify the crosslinking capacity (Figures S4-S6). Our results demonstrated that the 40 v/v% PEGDA exhibited an improved layer completeness and increased crosslinking thickness compared to the 20 v/v% and 60 v/v% formulations, when applying 2-mM/20-mM Ru/SPS, owing to the difference in optical properties of PEGDA at these concentrations. Similar conclusions were obtained in previous studies where 40 v/v% PEGDA possessed the minimum light attenuation at the wavelength from 400 to 800 nm.[15] However, the influence of PEGDA concentration on crosslinking thickness and layer completeness could not be observed in the inks supplemented with 4-mM/40-mM Ru/SPS. From these results

we obtained, the 40 v/v% PEGDA ink containing 2-mM/20-mM Ru/SPS was selected to be applied in the following printing sessions, providing better printability and crosslinking performances, as well as keeping the photoinitiator at a lower concentration.

Ponceau 4R, a synthetic food dye,[16] was added as a photoabsorber to limit light penetration depth, thereby preventing over-curing of the ink and facilitating the fabrication of structures with intricate internal geometries.[17] The absorbance spectrum of Ponceau 4R is identified to encompass visible-light wavelengths and has a maximum absorption at 508 nm,[18] suggesting it can be a strong photoabsorber candidate in our visible light-based printing system. Moreover, its cytocompatibility has been proven in our previous study, where the addition of Ponceau 4R did not have any negative effect on the encapsulated cells.[11] Indeed, we observed the reduced curing size and crosslinking thickness in the inks with higher photoabsorber concentrations, suggesting that Ponceau 4R successfully controlled the optical penetration length. In addition, the pixel size revealed by the microscope image in Figure S6b was 78 μm, which was dependent on the resolution of the smartphone-powered projector and the specifics of the optical system. The original projected size of the the smartphone-powered projector (G6S DLP Pocket Projector/Mini Projector) was 465 × 234 mm with the resolution of 954 × 480 pixels, which resulted in the original pixel size of 487.5 μm. Given the 10-fold demagnification of the optical system on the printer, approximately 49 μm was determined as the theoretical pixel size at the vat. While the actual pixel size in the printed constructs was slightly enlarged likely as a consequence of the diffusion of chemical species and/or the light scattering/diffraction, it was still deemed decently small enough to suit majority of the intended applications.

To further explore the capability of this smartphone-enabled printer to fabricate structures with internal cavities and investigate how the photoabsorber affected printability, 40 v/v% PEGDA (M_w = 575 Da), 2-mM/20-mM Ru/SPS, and photoabsorber at 1.0 wt.% or 2.5 wt.% were utilized in subsequent studies (Figure S7). The ink containing 1.0 wt.% (2×) photoabsorber was employed to print constructs with 300 μm of layer thickness under 30 s of exposure time. By contrast, the printing parameter was changed to 100 μm of layer thickness with the same exposure time when the photoabsorber concentration was increased to 2.5 wt.% (5×). Hollow structures printed with the ink containing 2.5 wt.% (5×) photoabsorber achieved longer square length (2 mm), thinner wall thickness (1.5 mm), and smaller layer depth (0.4 mm), gaining increased precision. Constructs containing embedded cylindrical channels of 1-mm-diameter were then printed (Figure S8). As the layer thickness was reduced using the ink added with more photoabsorber, the channel presented higher circularity, demonstrating better geometric fidelity as compared to the original model.

To illustrate the versatility of the smartphone-enabled DLP printing system, we also investigated 3D printing with multiple types of materials. With the commercial resin, we printed a series of 3D macroscopic objects at a speed of 32 μm s^{-1}, including the Chichen Itza Pyramid of 0.7 cm in height, the Medieval Tower of 2 cm in height, the Eiffel Tower of 2.25 cm in height, the Shanghai Oriental Pearl Tower of 2.25 cm in height, and the Tower of Babylon of 2.25 cm in height, as shown in Figure 3a. We further investigated whether the 3D constructs fabricated with our smartphone-enabled DLP printer could possibly compete with the printing achieved with the commercial SLA printer ($1,295,

Moai SLA 3D Printer, Peopoly). As shown in Figure S9, using the commercial resin (Photocentric Daylight Firm Resin, MatterHackers), the Shanghai Oriental Pearl Tower was printed with 2.25 cm of height in 16 min (23 μm s^{-1}) by the smartphone-enabled DLP system. However, the same structure was fabricated in 9 h at 0.69 μm s^{-1} by the SLA printer with the UV-curable resin (Moai Tough Resin, Peopoly). These results suggested that the smartphone-enabled DLP printer provided a time-saving and cost-effective source for 3D printing in comparison to commercial counterparts, although it presented a slightly reduced resolution as a compromise of its advantages. For instance, the hollow structure in the middle part of the Shanghai Oriental Pearl Tower could be observed in the commercial SLA-printed construct, while missed in the tower fabricated by the smartphone-enabled DLP printer. Further efforts could be devoted to further optimizing the various printing parameters, such as light intensity as well as exposure time and step size, to balance the pros and cons of our smartphone-enabled DLP printer.

To further validate the applicability of our platform, 40 v/v% PEGDA (M_w = 575 Da), 2-mM/20-mM Ru/SPS, and 2.5 wt.% photoabsorber was used to fabricate the 3D-printed constructs at the speed of 96 μm s^{-1}. As can be seen from Figure 3b, the Tower of Babylon showed 1 cm in height, half size of the US 1¢ coin. Particular emphasis was placed on successful generation of surface details at a resolution of approximately 100 μm on such a small construct by PEGDA. A similar result was observed for the chess piece (queen) characterized with fine tips (roughly 80 μm). Additionally, the PEGDA-printed gyroid structure showed a 2-mm pore size.[19] In Movie S2, the hollow helix channel with 1 mm of diameter was fully perfused with green dye, thereby indicating the potential of mimicking vascular structures with fabricated PEGDA constructs.

There are several types of hydrogels showing remarkable compatibility for 3D bioprinting. Gelatin methacryloyl (GelMA), as an important bioink possessing intrinsic bioactive moieties for cell adhesion, has been widely applied for both extrusion-based and light-assisted bioprinting.[20] We investigated a bioink based on 20 w/v% GelMA mixed with 4-arm PEG-acrylate (1 w/v%) to facilitate printability.[21] Using this approach, human organ analogues, such as the nose, ear, kidney, heart, and brain, were printed at the speed of 10 μm s^{-1} (Figure 3c). Detailed comparisons between 3D models and 3D-printed organ-analogues confirmed that similar surface morphologies were observed for the nose and ear constructs. However, complex high-resolution external surface features in the kidney, the heart, and the brain were slightly more difficult to achieve, such as the coronary vessels on the exterior surface of the heart and the multiple surface folds of the brain cortex.

Another hydrogel, allylated gelatin (GelAGE) synthesized from gelatin by reacting with allyl glycidyl ether, relies on the thiol–ene chemistry and offers additional advantages of rapid reaction kinetics in free-radical polymerization.[22] GelAGE has been previously reported as a platform bioink for DLP bioprinting as well as extrusion-based bioprinting, presenting high shape fidelity as well as high cell viability.[23] Results in Figure 3d indicated that the organ-analogues including the nose and the ear, a gyroid structure, and an interwoven mesh pattern were successfully printed with 20 w/v% GelAGE, 120-mM 1,4-dithiothreitol (DTT), 2-mM/20-mM Ru/SPS, and 1.0 wt.% photoabsorber, at the speed of 10 μm s^{-1}. The printed nose showed an identical shape to the 3D model. Moreover,

the intertwined woven mat struts were also successfully fabricated, suggesting that high shape fidelity could be obtained in solid hydrogel printing. We then further investigated the printing capability of sophisticated designs include an ear-shape construct and a porous gyroid scaffold. The shape of the ear was achieved but distinct surface details were missed, and staggered pores of the gyroid were only partially reproduced. One of the major hurdles in hydrogel-based 3D printing is the insufficient mechanical properties of most hydrogel-based inks, which result in the lack of ability to build self-supporting constructs and the limited shape fidelity during and/or after 3D printing.[24] Overall, this platform allowed utilization of a wide variety of commercial resins and bioinks (both of synthetic and natural origins), providing convenience for 3D printing/bioprinting with sophisticated shapes and internal structures.

It is well-established that 3D printing/bioprinting is essential for individual patient anatomy-inspired fabrication, enabling the possibilities of patient-specific treatments.[25] For instance, a number of surgical implants used to repair human injuries have been printed using the DLP approach with biodegradable or non-degradable materials, including ceramics, metals, and polymers.[26] More importantly, 3D-printed implants can be designed to directly match the anatomical shape of defects in a patient-customizable way with the aid of medical scanning profiles.[27] Therefore, being able to reconstruct complex structures or human tissues, using a portable form-factor combined with fast-printing capacity, the smartphone-enabled DLP 3D printer is potentially an ideal tool for the clinical applications. As a proof-of-concept study, we herein fabricated an implant with specific customized anatomic shape and size for a femoral condyle defect (Figure 4a). To replicate the geometry and the microarchitecture of the bone, structures containing irregular pores were designed based on the reaction-diffusion model.[28] With the assistance of this design principle, we printed a bone implant containing an irregular porous architecture to emulate the spongy structure of native bone. Finally, the fabricated construct was implanted into a cubic-shaped ex vivo pig femoral condyle defect (tissue obtained from local butcher), with 8 mm on each side. This approach enabled the construction of personalizable orthopedic solutions, which will likely enable additional possibilities in developing tissue implants, such as dental prostheses implants, knee or hip implants, and patient-specific mandibular implants in traumatic surgery.

We subsequently explored additional biomedical applications of our smartphone-enabled DLP printer for in situ bioprinting, defined as bioprinting directly on the living tissues.[29] As a proof-of-concept demonstration, a piece of porcine muscle (from the local butcher) was fixed onto the build platform with Vetbond Tissue Adhesive (3M), and then the build platform was lowered into the vat to a suitable distance where the muscle surface could be introduced into the bioink and reach the printing position (Figure 4bi). Using a bioink consisting of 10 w/v% GelMA, 2-mM/20-mM Ru/SPS, and C2C12 cells (8×10^6 cells mL^{-1}), in situ bioprinting was conducted with the specific anatomical shape of the injured area and a total thickness of 1 mm in 60 s. The result revealed that the site of injury on the porcine muscle was well-complemented by the printed bulk hydrogel scaffold of 1-mm depth and 4-mm diameter (Figure 4bii). The cross-sectional image confirmed the printed cell-laden hydrogel was retained in the host tissue (Figure 4biii), where the bulk hydrogel containing green fluorescent protein (GFP)-labeled C2C12 cells was connected to the surrounding tissues closely in the boundaries. It must be mentioned that most of the

bioprinted C2C12 cells were viable (>98% viability) from day 1 to day 14 according to live/dead analyses (Figure 4c). This result is consistent with the observation from previous studies regarding the safety of photopolymerization of GelMA, facilitated by the visible light and Ru/SPS photoinitiator.[9a, 30] Therefore, this demonstrates significant potential for applying our portable smartphone-enabled DLP printer as an enabling technology for future in vivo bioprinting.

There has been a large number of cases where failure to access advanced 3D printing technologies are present, considering the need for specialized facilities and highly trained technicians who are familiar with both 3D model designs and printing. In recognition of this shortcoming in resource-limited settings, the high-quality camera on the smartphone was utilized as an enabling sensing module for a 3D scanning smartphone App integrated into the printing workflow. It offered great opportunity for precisely obtaining shapes of target objects and printing customized samples in a rapid yet effort-minimized manner, either for individualized or medical 3D printing applications. As illustrated in Figure 5a, a set of photos of the object when taken from various angles using the 3D scanning App (e.g., Qlone, available for both Android and iOS smartphones) were used to generate a reconstructed 3D model, which was subsequently exported as an STL format required for 3D printing by taking advantage of our customized printing App.

Another interesting modification of the developed smartphone-enabled printer was its scalable capacity, endued into the printer via adjusting the positions of lenses slotted into the system, resulting in 1- to 1.5-times magnifications of the printed samples (Figure 5b). It is important to highlight that the light intensity was increased when moving the lens closer to the vat. Therefore, to achieve the comparable printing results of 40 v/v% PEGDA (M_W = 575 Da) and 2-mM/20-mM Ru/SPS illustrated in Figure 5b, the crosslinking time was determined at 15 s, 10 s, or 5 s at Level 1, Level 2, or Level 3, respectively. In Figure 5c, a rabbit-shaped object and a femoral condyle (obtained from local butcher) with different sizes were first scanned, then reconstructed, and finally printed using a commercial resin within 5 min. Favorable similarities of overall morphologies were presented between the printed constructs and their respective original objects. Some detailed features on the surfaces could not be fully resolved, such as those on the nose and eyes of the rabbit, and ligaments of the femoral condyle. It was likely affected by the curing depth of the resin as well as several additional printing parameters, including step size and exposure light dosage. Overall, the ease in obtaining 3D models from the 3D scanning smartphone App, adjustable structural size, and user-friendly operation platform were all converged into the smartphone-enabled DLP printing system. The usability of this unique platform in resource-limited and on-demand settings, such as those with limited infrastructures and human resources, or those requiring time-sensitivity at the bedside, will bring promising opportunities for its broadened application.[31]

In summary, we developed an unprecedented portable DLP 3D printer based on a smartphone-powered projector as well as a customized touchscreen smartphone App, enabling us to achieve printing of 3D constructs in minutes using standardized printing process with a high level of automation and accuracy. We highlighted that this printing platform featured significant advantages, including portability, modularity, an easy-to-use

interface, as well as the integration of the 3D scanning smartphone App. The ability of printing with versatile materials covering commercially available hard resins and soft hydrogels was demenstrated, satisfying a broad range of applications. This portable printer was also proven to be suitable in resource-limited settings, especially by utilizing the 3D object-scanning App on the smartphone in conjunction with our own custom-written printing App, minimizing the knowledge required for designing 3D computer-aided design models and for operating the 3D printer. We reasonably envision the significant potential of our smartphone-enabled portable DLP printer in various fields such as medicine, biomedicine, home, and education, among others.

Supplementary Material

Refer to Web version on PubMed Central for supplementary material.

Acknowledgments

The authors gratefully acknowledge funding from the National Institutes of Health (R21EB026175, R21EB025270, R00CA201603, R01EB028143), the National Science Foundation (CBET-EBMS-123859), and the Brigham Research Institute. K.S.L. acknowledges funding by New Zealand Health Research Council (Emerging Researcher First Grant – 15/483, Sir Charles Hercus Health Research Fellowship – 19/135) and Royal Society of New Zealand (Marsden Fast Start – MFP-UOO1826). T.W. acknowledges funding from Royal Society of New Zealand (Rutherford Discovery Fellowship – RDF-UOO1204) and Ministry for Business, Innovation & Employment (UOOX1407).

References

[1]. a) Fu K, Yao Y, Dai J, Hu L., Adv. Mater 2017, 29;b) Truby RL, Lewis JA, Nature 2016, 540, 371; [PubMed: 27974748] c) Liaw CY, Guvendiren M., Biofabrication 2017, 9, 024102; [PubMed: 28589921] d) Ma X, Liu J, Zhu W, Tang M, Lawrence N, Yu C, Gou M, Chen S., Adv. Drug. Deliv. Rev 2018, 132, 235. [PubMed: 29935988]

[2]. Valot L, Martinez J, Mehdi A, Subra G., Chem. Soc. Rev2019, 48, 4049. [PubMed: 31271159]

[3]. a) Quesada-González D, Merkoçi A., Biosensors and Bioelectronics 2017, 92, 549; [PubMed: 27836593] b) Breslauer DN, Maamari RN, Switz NA, Lam WA, Fletcher DA, PLoS One 2009, 4, e6320. [PubMed: 19623251]

[4]. Kühnemund M, Wei Q, Darai E, Wang Y, Hernández-Neuta I, Yang Z, Tseng D, Ahlford A, Mathot L, Sjöblom T., Nat. Commun2017, 8, 1. [PubMed: 28232747]

[5]. Azzarelli JM, Mirica KA, Ravnsbaek JB, Swager TM, Proc. Natl. Acad. Sci. U S A2014, 111, 18162. [PubMed: 25489066]

[6]. a) Yan X, Gu P., Computer-aided design 1996, 28, 307;b) Lim KS, Galarraga JH, Cui X, Lindberg GCJ, Burdick JA, Woodfield TBF, Chem. Rev 2020, 120, 10662. [PubMed: 32302091]

[7]. Li W, Mille LS, Robledo JA, Uribe T, Huerta V, Zhang YS, Adv. Healthc. Mater2020, 9, e2000156. [PubMed: 32529775]

[8]. a) Hribar KC, Soman P, Warner J, Chung P, Chen S., Lab Chip 2014, 14, 268; [PubMed: 24257507] b) Ng WL, Lee JM, Zhou M, Chen YW, Lee KA, Yeong WY, Shen YF, Biofabrication 2020, 12, 022001; [PubMed: 31822648] c) Kim SH, Yeon YK, Lee JM, Chao JR, Lee YJ, Seo YB, Sultan MT, Lee OJ, Lee JS, Yoon SI, Hong IS, Khang G, Lee SJ, Yoo JJ, Park CH, Nat. Commun 2018, 9, 1620; [PubMed: 29693652] d) Kuang X, Wu J, Chen K, Zhao Z, Ding Z, Hu F, Fang D, Qi HJ, Sci. Adv 2019, 5, eaav5790; [PubMed: 31058222] e) Patel DK, Sakhaei AH, Layani M, Zhang B, Ge Q, Magdassi S., Adv. Mater 2017, 29.

[9]. a) Wang Z, Kumar H, Tian Z, Jin X, Holzman JF, Menard F, Kim K., ACS Appl. Mater. Interfaces 2018, 10, 26859; [PubMed: 30024722] b) Zheng Z, Eglin D, Alini M, Richards GR, Qin L, Lai Y., Engineering 2020.

[10]. Tumbleston JR, Shirvanyants D, Ermoshkin N, Janusziewicz R, Johnson AR, Kelly D, Chen K, Pinschmidt R, Rolland JP, Ermoshkin A, Samulski ET, DeSimone JM, Science2015, 347, 1349. [PubMed: 25780246]

[11]. Lim KS, Levato R, Costa PF, Castilho MD, Alcala-Orozco CR, van Dorenmalen KMA, Melchels FPW, Gawlitta D, Hooper GJ, Malda J, Woodfield TBF, Biofabrication2018, 10, 034101. [PubMed: 29693552]

[12]. a) Von Freymann G, Ledermann A, Thiel M, Staude I, Essig S, Busch K, Wegener M., Adv. Funct. Mater, 2010, 20, 1038;b) Wilts BD, Zubiri BA, Klatt MA, Butz B, Fischer MG, Kelly ST, Spiecker E, Steiner U, Schröder-Turk GE, Sci. Adv 2017, 3, e1603119; [PubMed: 28508050] c) Torres-Rendon JG, Femmer T, De Laporte L, Tigges T, Rahimi K, Gremse F, Zafarnia S, Lederle W, Ifuku S, Wessling M., Adv. Mater 2015, 27, 2989. [PubMed: 25833165]

[13]. Ahn D, Stevens LM, Zhou K, Page ZA, ACS Cent. Sci2020, 6, 1555. [PubMed: 32999930]

[14]. a) Wu J, Zhao Z, Kuang X, Hamel CM, Fang D, Qi HJ, Multifunctional Materials 2018, 1, 015002;b) Miri AK, Nieto D, Iglesias L, Goodarzi Hosseinabadi H, Maharjan S, Ruiz-Esparza GU, Khoshakhlagh P, Manbachi A, Dokmeci MR, Chen S., Adv. Mater 2018, 30, 1800242;c) Gungor-Ozkerim PS, Inci I, Zhang YS, Khademhosseini A, Dokmeci MR, Biomater. Sci 2018, 6, 915. [PubMed: 29492503]

[15]. Guo J, Zhou M, Yang C., Sci. Rep2017, 7, 7902. [PubMed: 28801653]

[16]. Amchova P, Kotolova H, Ruda-Kucerova J., Regul. Toxicol. Pharmacol2015, 73, 914. [PubMed: 26404013]

[17]. a) Grigoryan B, Paulsen SJ, Corbett DC, Sazer DW, Fortin CL, Zaita AJ, Greenfield PT, Calafat NJ, Gounley JP, Ta AH, Science 2019, 364, 458; [PubMed: 31048486] b) Zhang YF, Ng CJX, Chen Z, Zhang W, Panjwani S, Kowsari K, Yang HY, Ge Q., Adv. Mater. Technol 2019, 4, 1900427.

[18]. Chanlon S, Joly-Pottuz L, Chatelut M, Vittori O, Cretier J, Food Compos J. Anal2005, 18, 503.

[19]. Grigoryan B, Paulsen SJ, Corbett DC, Sazer DW, Fortin CL, Zaita AJ, Greenfield PT, Calafat NJ, Gounley JP, Ta AH, Johansson F, Randles A, Rosenkrantz JE, Louis-Rosenberg JD, Galie PA, Stevens KR, Miller JS, Science2019, 364, 458. [PubMed: 31048486]

[20]. a) Ying G, Jiang N, Yu C, Zhang YS, Biodes. Manuf 2018, 1, 215;b) Maharjan S, Alva J, Cámara C, Rubio AG, Hernández D, Delavaux C, Correa E, Romo MD, Bonilla D, Santiago ML, Matter 2021, 4, 217. [PubMed: 33718864]

[21]. Sheth S, Barnard E, Hyatt B, Rathinam M, Zustiak SP, Front. Bioeng. Biotechnol2019, 7, 410. [PubMed: 31956651]

[22]. a) Hoyle CE, Lowe AB, Bowman CN, Chem. Soc. Rev 2010, 39, 1355; [PubMed: 20309491] b) Soliman BG, Lindberg GCJ, Jungst T, Hooper GJ, Groll J, Woodfield TBF, Lim KS, Adv. Healthc. Mater 2020, 9, e1901544. [PubMed: 32323473]

[23]. Bertlein S, Brown G, Lim KS, Jungst T, Boeck T, Blunk T, Tessmar J, Hooper GJ, Woodfield TBF, Groll J., Adv. Mater2017, 29.

[24]. Duan B., Ann. Biomed. Eng2017, 45, 195. [PubMed: 27066785]

[25]. a) Heller M, Bauer HK, Goetze E, Gielisch M, Roth KE, Drees P, Maier GS, Dorweiler B, Ghazy A, Neufurth M, Muller WE, Schroder HC, Wang X, Vahl CF, Al-Nawas B., Int. J. Comput. Dent 2016, 19, 323; [PubMed: 28008429] b) Witowski J, Sitkowski M, Zuzak T, Coles-Black J, Chuen J, Major P, Pdziwiatr M., Int. J. Comput. Assist. Radiol. Surg 2018, 13, 1473. [PubMed: 29790077]

[26]. Zhang J, Hu Q, Wang S, Tao J, Gou M., Int. J. Bioprint2020, 6, 242. [PubMed: 32782984]

[27]. a) Anssari Moin D, Hassan B, Wismeijer D., Clin. Oral Implants Res 2017, 28, 668; [PubMed: 27114184] b) Kuhnt T, Marroquin Garcia R, Camarero-Espinosa S, Dias A, Ten Cate AT, van Blitterswijk CA, Moroni L, Baker MB, Biomater. Sci 2019, 7, 4984. [PubMed: 31667486]

[28]. Velasco MA, Lancheros Y, Garzón-Alvarado DA, J. Comput. Des. Eng2016, 3, 385.

[29]. a) Singh S, Choudhury D, Yu F, Mironov V, Naing MW, Acta biomater 2020, 101, 14; [PubMed: 31476384] b) Ahadian S, Khademhosseini A., Biodes. Manuf 2018, 1, 157; [PubMed: 30906618] c) Wu Y, Ravnic DJ, Ozbolat IT, Trends Biotechnol 2020, 38, 594; [PubMed: 32407688] d) Murphy SV, De Coppi P, Atala A., Nat. Biomed. Eng 2020, 4, 370; [PubMed: 31695178] e)

Hakimi N, Cheng R, Leng L, Sotoudehfar M, Ba PQ, Bakhtyar N, Amini-Nik S, Jeschke MG, Gunther A., Lab Chip 2018, 18, 1440. [PubMed: 29662977]

[30]. Lim KS, Schon BS, Mekhileri NV, Brown GC, Chia CM, Prabakar S, Hooper GJ, Woodfield TB, ACS biomaterials science & engineering2016, 2, 1752. [PubMed: 33440473]

[31]. Drain PK, Hyle EP, Noubary F, Freedberg KA, Wilson D, Bishai WR, Rodriguez W, Bassett IV, Lancet Infect. Dis2014, 14, 239. [PubMed: 24332389]

[32]. a) Yue K, Trujillo-de Santiago G, Alvarez MM, Tamayol A, Annabi N, Khademhosseini A., Biomaterials 2015, 73, 254; [PubMed: 26414409] b) Gong J, Schuurmans CC, van Genderen AM, Cao X, Li W, Cheng F, He JJ, López A, Huerta V, Manríquez J., Nat. Commun 2020, 11, 1. [PubMed: 31911652]

[33]. Yoon HJ, Shin SR, Cha JM, Lee SH, Kim JH, Do JT, Song H, Bae H., PLoS One2016, 11, e0163902. [PubMed: 27723807]

[34]. Bertlein S, Brown G, Lim KS, Jungst T, Boeck T, Blunk T, Tessmar J, Hooper GJ, Woodfield TB, Groll J., Adv. Mater2017, 29, 1703404.

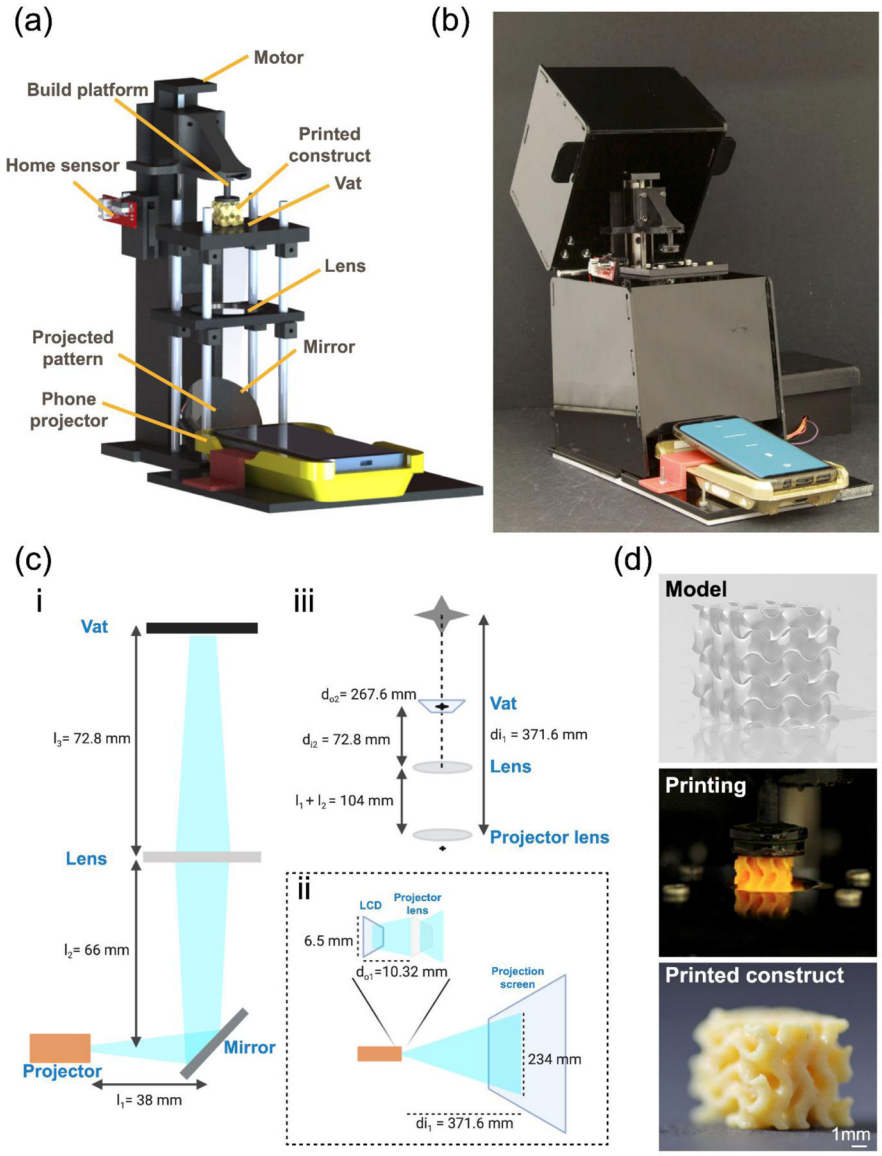

Figure 1.

Smartphone-enabled DLP printer. (a, b) Schematic and photograph, respectively, of the printing system. (c) Diagrams of the optical system: i, the optical relationship between the projector, the mirror, the lens, and the vat; ii, the optical path inside the smartphone-powered projector; iii, schematic shows the calculation of magnification between the projector lens and the vat. (d) Example of a gyroid printing from the 3D model to the printed construct.

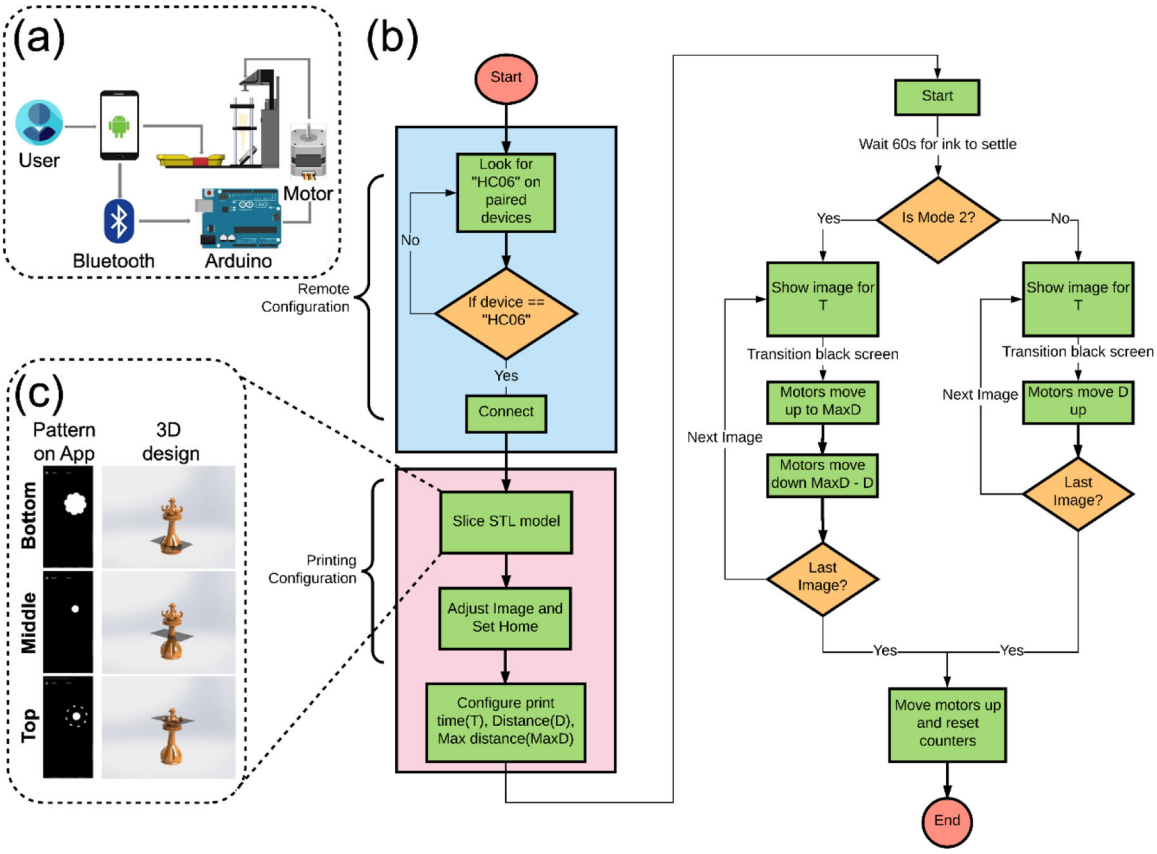

Figure 2.

Communication and algorithm of the printing App. (a) Communication between the user and the printer. (b) Flow chart of the algorithm. (c) Examplary sliced patterns of a 3D chess piece shown on the smartphone. T, time; D, Distance.

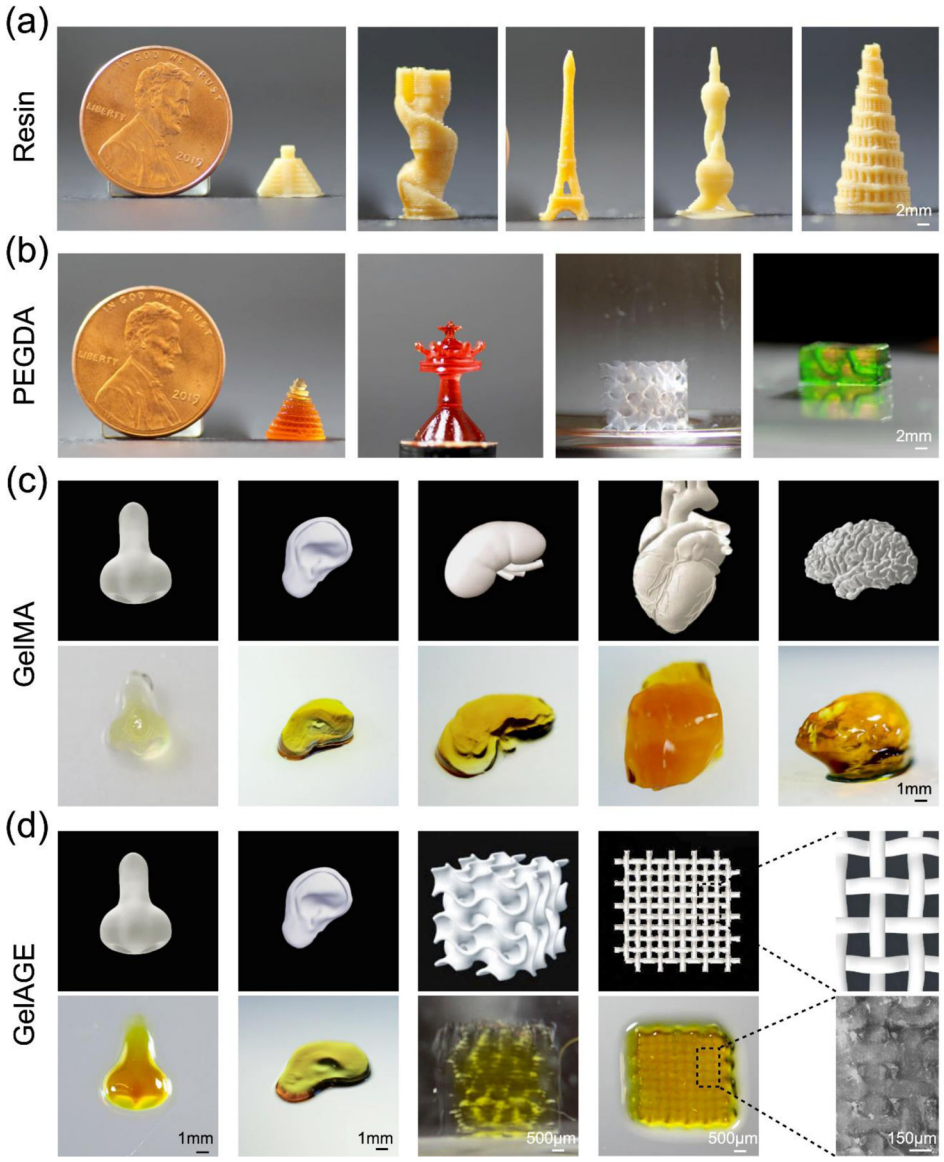

Figure 3.

3D constructs printed with the smartphone-enabled DLP printer. (a) Constructs printed with commercial resin at the speed of 32 μm s^{-1}. (b) Constructs printed with 40 v/v% PEGDA (M_w = 575 Da) at the speed of 96 μm s^{-1}. (c) Organ-analogues printed with 20 w/v% GelMA + 1 w/v% 4-arm PEG-acrylate at the speed of 10 μm s^{-1}. (d) Organ-analogues printed with 20 w/v% GelAGE +120-mM DTT, at the speed of 10 μm s^{-1}.

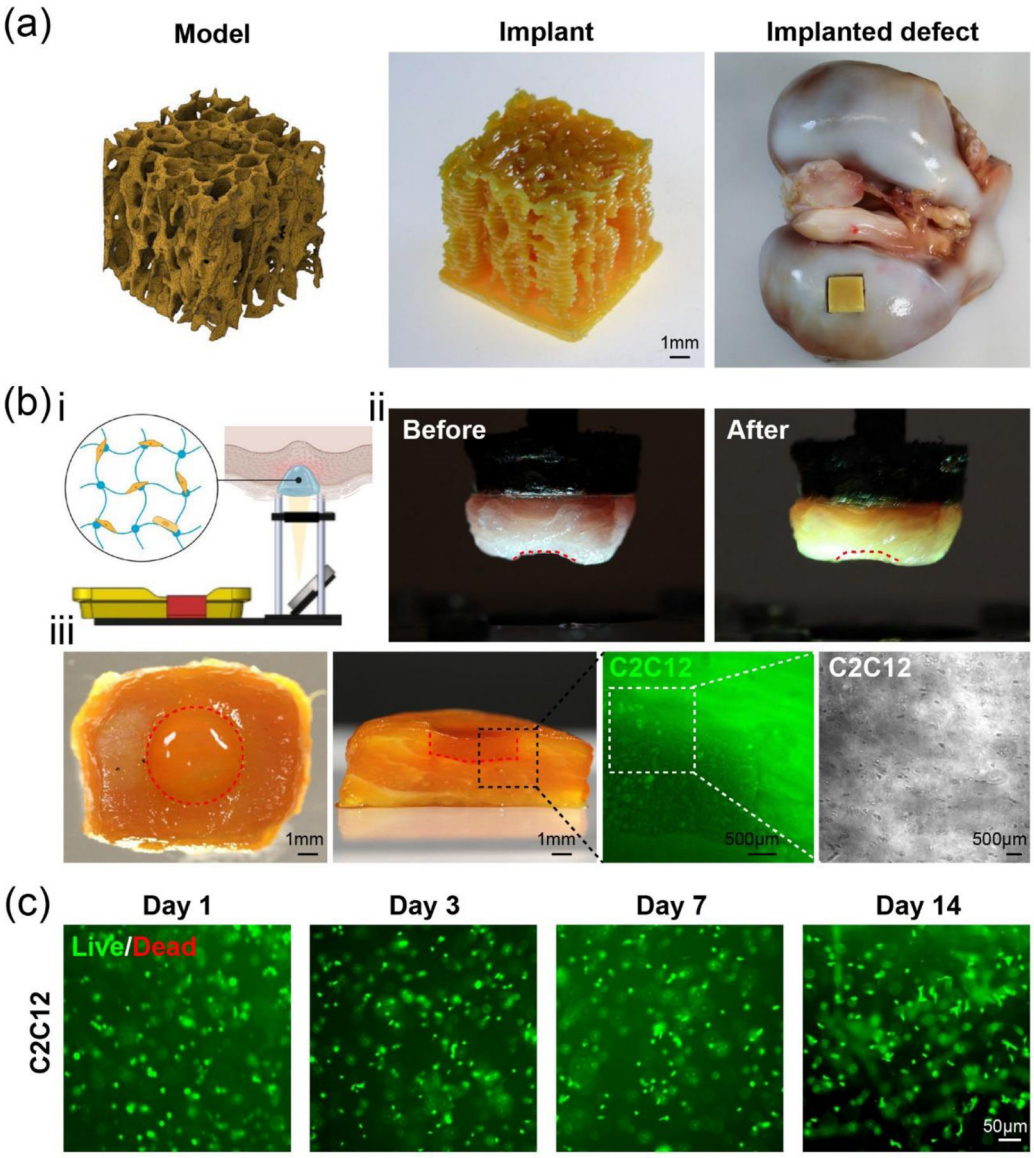

Figure 4.

Biomedical applications of the smartphone-enabled DLP printer. (a) A porous bone implant-mimic printed using commercial resin. (b) In situ bioprinting with 10 w/v% GelMA: i, diagram of the bioprinting setup on a piece of pork muscle with a defect site; ii, photographs of the pork muscle before and immediately after bioprinting, where the red dashed lines indicate the boundaries of the initial muscle defect; iii, top and cross-sectional views of the same piece post-bioprinting, followed by enlarged images showing C2C12 cells (green) encapsulated in the bioprinted 10 w/v% GelMA tissue construct in the defect area. The rightmost panel presents the bright-field micrograph of C2C12 cells encapsulated in the printed hydrogel, which was captured immediately after in situ bioprinting. The boundaries of the injured area are indicated by the red dashed line. (c) Live/dead images of C2C12 cells within GelMA at 1, 3, 7, and 14 days after bioprinting.

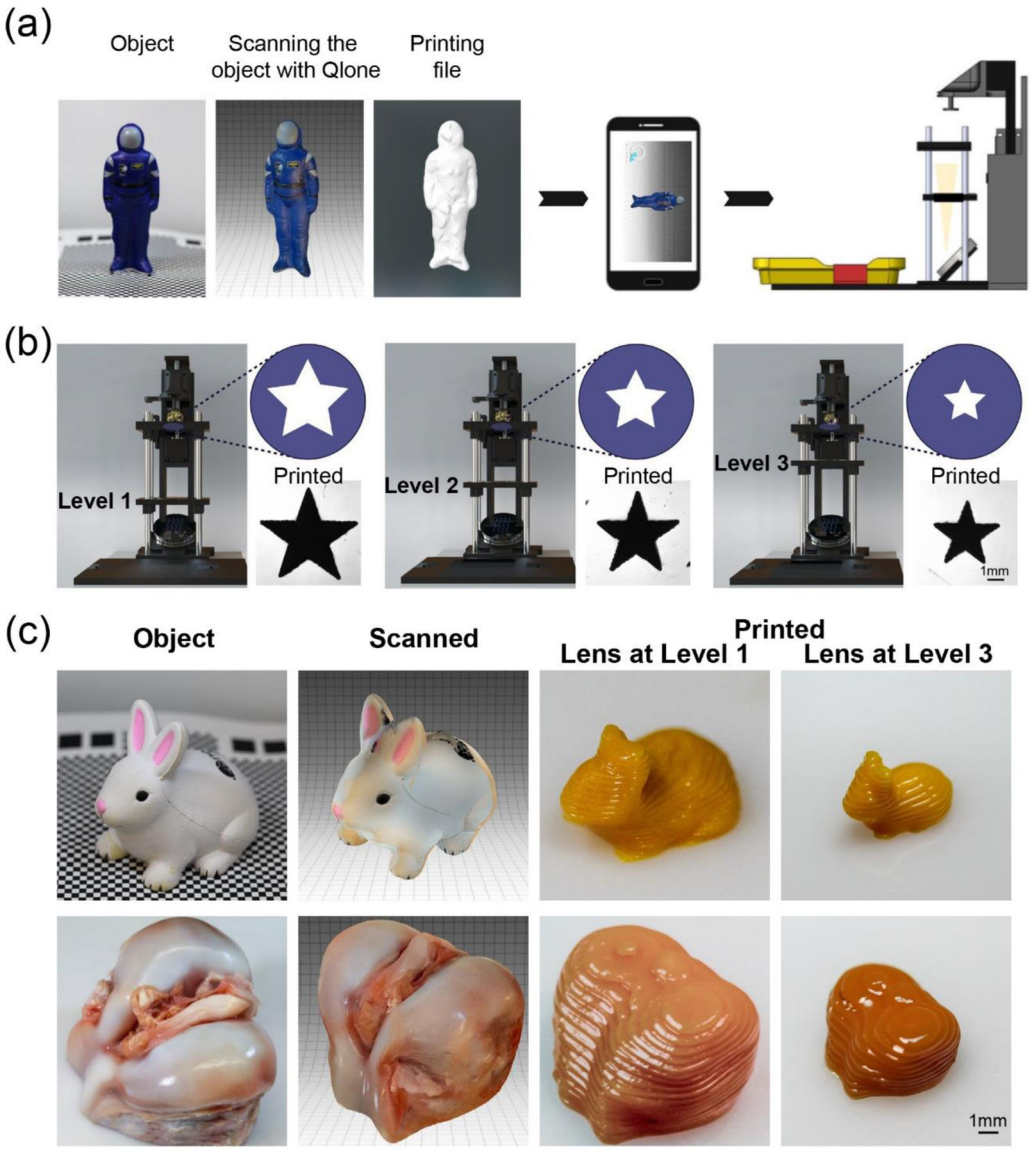

Figure 5.

Integration of the smartphone 3D scanning App. (a) Scheme showing printing with the model obtained from the 3D scanning App. (b) Various magnifications achieved from 1.5 to 1.0 times through adjusting the level of focusing lens from Level 1 to Level 3. Images in right-bottom corners present printed constructs exposed to the same projecting pattern that was passed through different focusing lenses. (c) 3D-printed bunny toys and femoral condyle constructs with Level 1- to Level 3-magnifications.